Complexity Project: The Oslo Model

CID: 01413021

17th February, 2020

Abstract: The aim of this report is to implement the Oslo model and demonstrate its self-organised criticality phenomena. System sizes L = 4, 8, 16, 32, 64, 128, 256, 512 were used for up to 10^6 runs. With this model, the height of the pile displayed self-organised criticality and a scaling function was identified to perform a data collapse.

The avalanche-size probability was found and used to perform a data collapse with a scaling function, giving the parameters $D = 2.18 \pm 0.01$ and $\tau_s = 1.53 \pm 0.01$. Finally, the k^{th} moment of the avalanche size was found and used to estimate the scaling function parameters, giving the new values: $D = 2.15 \pm 0.01$ and $\tau_s = 1.58 \pm 0.01$, which is consistent with the previous values with a 1.4% and 3.3% deviation, respectively.

Word count: 2481 words in report (excluding front page, figure captions, table captions, acknowledgement and bibliography).

1 Introduction

Experiments of adding grains to a ricepile shows that the system demonstrates self-organised criticality (SOC) [1]. The simple Bak-Tang-Wiesenfeld (BTW) model has successfully modelled other systems displaying SOC, such as a pile of sand grains. However, for the ricepile experiment the slope have spatial and temporal variations, making the BTW model too simple. To account for these fluctuations, Christensen *et al.* introduced the Oslo model [2], which is identical to the BTW-model, except that the slope may change when a site topples.

The Oslo model is one of the simplest and most robust systems displaying SOC. Despite its simple algorithm, the model has many rich non-trivial features that can not be solved analytically. The aim of this project is to investigate the behaviour of the SOC system and identify features such as scaling and data collapse, using a computational implementation of the model.

1.a Oslo Model Algorithm

Consider a one-dimensional lattice of L sites, i = 1,2,3,...,L. The slope at site i is defined as $z_i = h_i - h_{i+1}$, where h_i is the height of the pile. Each site is assigned a threshold slope z_i^{th} that can take the values 1 or 2. The system is driven by adding a grain at site i = 1. If $z_i > z_i^{th}$ site i relaxes by toppling the grain to site i + 1 for $1 < i < L$ giving the new slopes

$$z_i \to z_i - 2 \qquad \text{and} \qquad z_{i\pm1} \to z_{i\pm1} + 1. \tag{1}$$

If site i = L relaxes, the grain leaves the system. Whenever a site relaxes, a new threshold slope is assigned randomly using

$$z_i^{\text{th}} = \begin{cases} 1 & \textit{with probability } p \\ 2 & \textit{with probability } 1-p \end{cases} \tag{2}$$

In the Oslo model $p = 1/2$ [3]

1.b Implementation and Testing

The model was implemented in Python using the algorithm as described in [3]. To improve the efficiency, the sites being checked were limited to the adjacent sites after a site toppled. All sites that needed to be checked were added to a list and when there were no more sites to check the system was driven again. As the model is *Abelian*, the order of the supercritical sites that are relaxed are independent of the behaviour of model [4]. This method greatly reduces the computation time, compared to the naive implementation of checking every site.

To check that the model was working as expected, the height of the pile at $i = 1$ was measured for different probabilities. For p = 1, $\langle z \rangle = 1$, which from Equation 5 gives the expected height $\langle h \rangle = L$. For p = 0, $\langle z \rangle = 2$ making the expected height $2L$. The

	Height of pile		Cross-over time	
Probability	Measured	Expected	Measured	Expected
p = 0	64.0	64	528.0	528
p = 1	32.0	32	1056.0	1056
p = 1/2	53.88 ± 0.04	53.9	868.2 ± 43.2	528 <t_c<1056

Table 1: Measured steady state height of pile and cross-over time from the implementation of the Oslo model, compared to the expected results. The test was conducted for system size L = 32.

expected heights for p = 0.5 are given in [3]. The measured values are summarised in Table 1. The table also shows the measured cross-over time for different probabilities, which is consistent with the estimate later derived in Equation 8. Since the measured values agrees with the expected values, it can be assumed the model is working as intended.

2 The Height of the Pile

In this section, the height of the pile will be studied in detail for system sizes $L \in \{4, 8, 16, 32, 64, 128, 256, 512\}$.

2.a Height vs time

Figure 1 shows the height of the pile, $h(t; L)$ plotted against time for various system sizes. It illustrates the clear distinction between the transient and recurrent configurations of the model. The transient configurations are the increasing height region at the start, where grains are added to the system, without leaving the system. During this configuration, $h(t, L)$ is independent of system size and increases equally for all system sizes. Transient configurations are encountered at most once and are not accessible when the system has entered the recurrent configurations. The flat region represents the recurrent configurations, where the number of grains entering the system, equals the number of grains leaving the system. This is a steady state where the

$$\langle \text{influx} \rangle = \langle \text{outflux} \rangle. \tag{3}$$

In contrast to the transient configurations, the recurrent configurations can be revisited indefinitely.

2.b Scaling relation for L >>1

The height of the pile at time t can be found from summing up all the local slopes

$$h(t; L) = \sum_{i=1}^{L} z_i(t) = \frac{L}{L} \sum_{i=1}^{L} z_i(t) = L \left\langle z_i(t; L) \right\rangle . \tag{4}$$

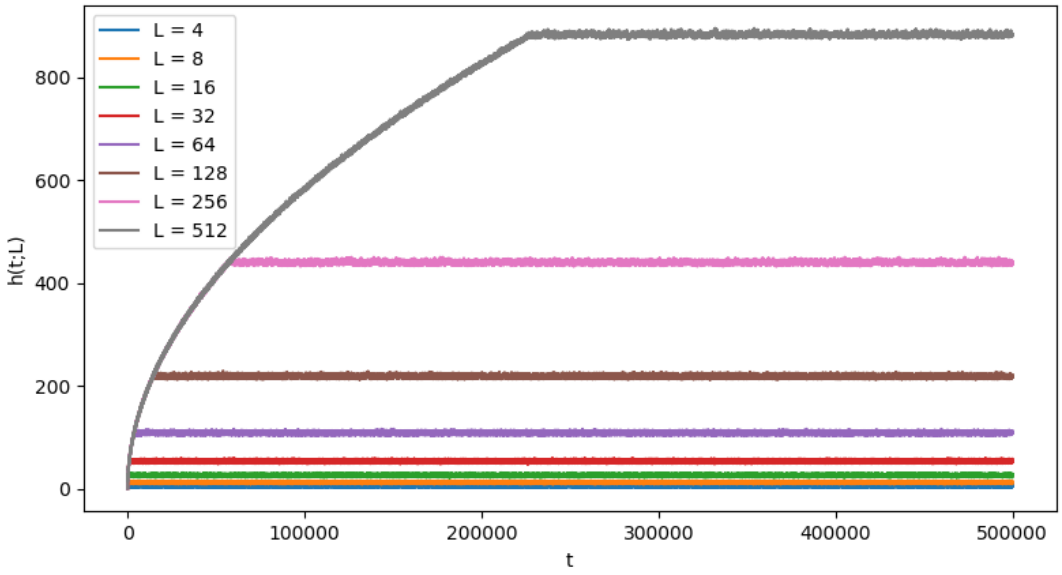

Figure 1: The height of the pile at time t, for various system sizes. The increasing region at at the start represents the transient configurations, while flat region represents the recurrent configurations.

For large system sizes in steady state, the average slope can be assumed to be constant for all L, as it becomes increasingly unlikely to deviate from the average slope from the Central Limit Theorem (CLT). Such that the height can be approximated for $L >> 1$ by

$$h(t; L) \approx \langle z \rangle L. \tag{5}$$

The crossover time, t_c, is defined as the number of grains in the system, before an added grain causes a grain to leave the system. The cross-over time is approximately equal to the number of grains in the system in steady state, from the relation in Equation 3. Therefore, t_c can roughly be estimated by considering a right-angled triangle, of height h(t ; L) and base length L, where its area is the cross-over time

$$\langle \ell_c(L) \rangle \approx \frac{L}{2} h(t; L) \approx \frac{L}{2} \langle z \rangle L \approx \frac{L^2 \langle z \rangle}{2} \tag{6}$$

such that the cross-over time scales as L^2 for large system sizes.

2.c Height and cross-over time scaling

From Equation 5, the height of the pile scales linearly with L, by assuming that $\langle z \rangle$ is constant and independent of system size L. The estimate of the cross-over time in Equation 6, can be refined by estimating the number of grains in the system with the equation

$$t_c(L) = \sum_{i=1}^{L} z_i \cdot i, \tag{7}$$

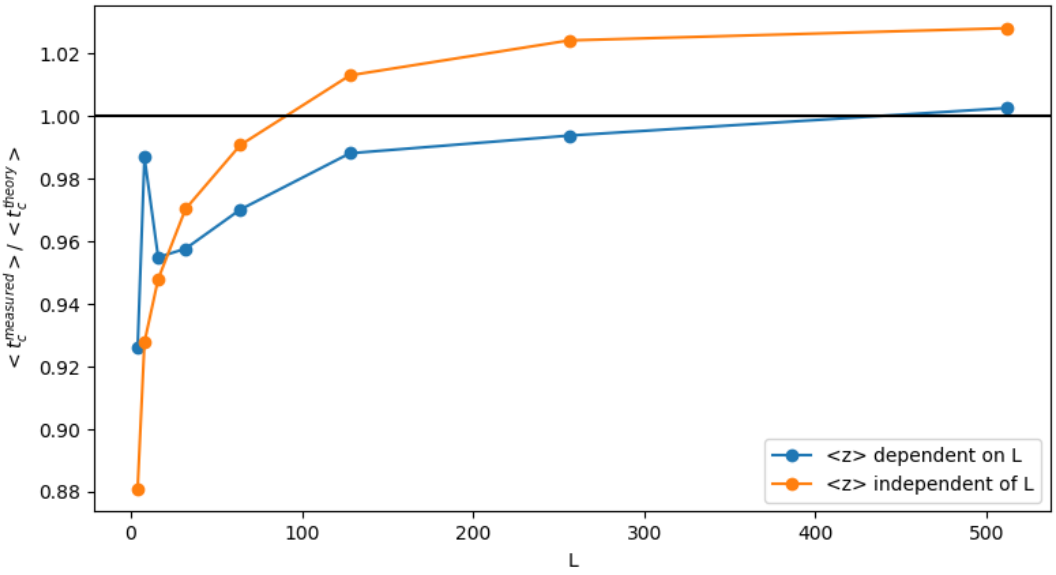

Figure 2: Ratio of the measured cross-over time, to the theoretical, plotted as a function of system size. The theoretical cross-over time have been calculated both using the average slope across all system sizes (z independent of L) and the average slope for each system size (z dependent on L).

given in [3]. To find the the scaling with L, the sum can be turned in to an expectation value

$$t_c(L) = \frac{L}{L}\sum_{i=1}^{L} iz_i = L\left\langle iz_i(L)\right\rangle .$$

assuming that that $\langle z_i\rangle$ is independent of position

$$\begin{aligned} t_c(L) &= L\left\langle z(L)\right\rangle \langle i\rangle \\ &= L\left\langle z(L)\right\rangle \frac{1}{L}\sum_{i=1}^{L} i \\ &= L\left\langle z(L)\right\rangle \frac{L(L+1)}{2L} \\ &= \frac{\langle z(L)\rangle}{2} L^2(1+\frac{1}{L}) \end{aligned}$$

Finally, assuming that the average slope is independent of system size, the average cross-over time can be estimated

$$\langle t_c\rangle = \frac{\langle z\rangle}{2} L^2(1+\frac{1}{L}) \tag{8}$$

where the $1/L$ term represents the corrections to scaling. To verify the relationship between $\langle t_c\rangle$ and L, Figure 2 shows L vs the ratio of the measured crossover time to the estimate in Equation 8, averaged over 20 models. The theoretical cross-over time, $\langle t_c^{theory}\rangle$,

is calculated both for the average slope across all system sizes, i.e assuming that $\langle z \rangle$ is independent of system size, and using the average for each system size, i.e assuming $\langle z \rangle$ is dependent on system size. The figure shows that the measured cross-over time lies closely to the desired line for large enough system sizes. The assumption that $\langle z \rangle$ is dependent on L gives the best estimate, which illustrates that the last assumption in Equation 8 causes a discrepancy from the measured values. This discrepancy arises from the fact that the assumption that $\langle z \rangle$ is independent of position is not valid at the boundaries, as the relaxation rules are different here. Consequently, $\langle z \rangle$ is dependent on L for finite system sizes [5].

2.d Height data collapse

With the knowledge of how $\langle t_c \rangle$ and $h(t, L)$ scales with L, a scaling function can be proposed

$$\tilde{h}(t; L) = L\mathcal{F}\left(t/L^2\right) \tag{9}$$

where $\tilde{h}(t; L)$ represents the average height for different realisations, which is used to smooth out the data. Once the system reaches the cross-over time, $h(t; L)$ tends to a constant, and so the scaling function $\mathcal{F}(x)$ must be constant for $t/L^2 >> 1$. For small arguments, the height increases with time and thus the scaling function has to follow a power law

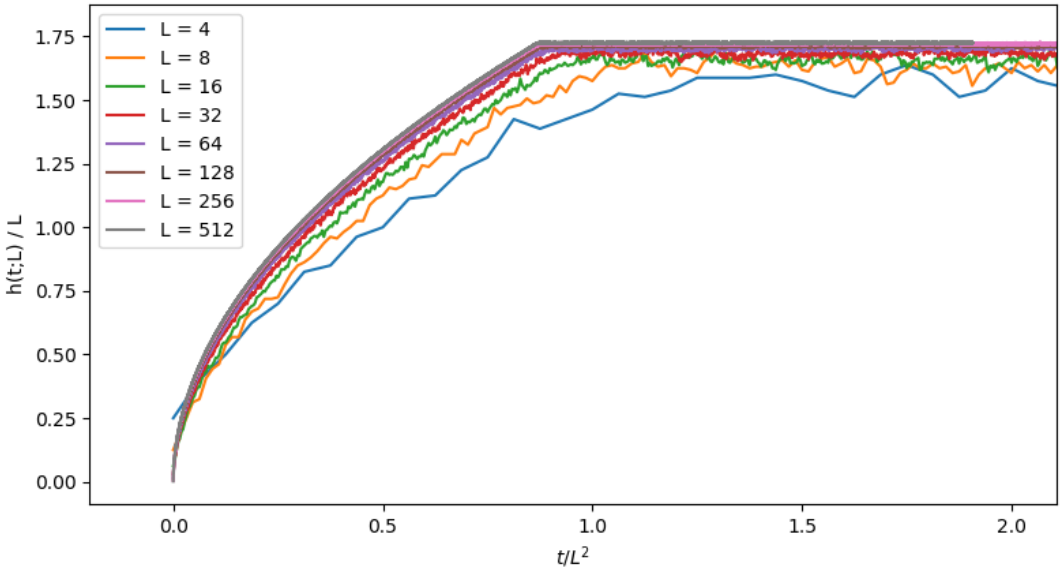

Figure 3: The height of the pile vs time, plotted using the scaling relation identified in Section 2d. For small system sizes, corrections to scaling can be seen in the deviation from the data collapse. The data have been averaged over 20 different realisations.

$$\mathcal{F}(x) \propto \begin{cases} \text{constant} & \text{x >>1.} \\ x^{\frac{1}{D}} & \text{x <<1} \end{cases} \tag{10}$$

where D is a constant. During the transient configurations no grains leave the system, and so $\mathcal{F}(x)$ has to be independent of system size L. Since $x = t/L^2$, the only value of D that causes L to cancel is $D = 2$. Thus for t/L^2<<1 the height scales as

$$\tilde{h}(t; L) \propto t^{\frac{1}{2}}. \tag{11}$$

This result was verified by finding the exponent in the transient region of $h(t; L)$, which agreed with the expected value of 0.5. Figure 3 shows the data collapse using the behaviour found above. The data has been smoothed out by averaging 20 simulations with different realisations. It illustrates that the scaling relationship works well for large system sizes, however for small values, corrections to scaling can be seen in the deviation from the collapsed larger system sizes.

2.e Corrections to scaling

To evaluate the corrections to scaling, the equation

$$\langle h(t; L)\rangle_t = a_0 L \left(1 - a_1 L^{-\omega_1} + a_2 L^{-\omega_2} + \ldots\right) \tag{12}$$

is used to model the heights [3], where $w_i > 0$ and a_i are constants. Neglecting higher order terms

$$\langle h(t; L)\rangle = a_0 L \left(1 - a_1 L^{-\omega_1}\right) \tag{13}$$

Note that $h(t; L)$ is only measured in the steady state where t>t_c. Rearranging and taking the log of both sides yields

$$\log\left(1 - \frac{\langle h(t; L)\rangle_t}{a_0 L}\right) = -\omega_1 \log L + \log a_1. \tag{14}$$

For the right value of a_0, a plot of $\log\left(1 - \langle h(t; L)\rangle_t / a_0 L\right)$ vs $\log L$ should yield a straight line. Therefore, the value of a_0 that gives the best linear fit can be used to estimate a_0. To make an initial guess of a_0, it can be noted that Equation 5 and 13 must tend to the same value as $L \longrightarrow \infty$, such that $a_0 \longrightarrow \langle z\rangle$. Therefore a_0 should be in the range of $1.5 < a_0 < 2$. Figure 4 shows the coefficient of determination, R^2 plotted for 10 different a_0 values. Using a refined range of $1.7 < a_0 < 1.8$, the a_0 that maximises R^2 are found to be $a_0 = 1.736 \pm 0.007$. It is possible to use more values of a_0, but it would not increase the accuracy as there are uncertainty in the $\langle h(t; L)\rangle_t$ data. Using this value, w_1 can be found from the gradient of Equation 14. The measured values and associated linear fit have been plotted in Figure 5, where w_1 were found to be $w_1 = 0.560 \pm 0.006$.

2.f Standard deviation scaling

Figure 6 shows the standard deviation of the height as a function of the system size L, plotted on a log-log scale. Since the plot yields a straight line, we can assume that σ_h

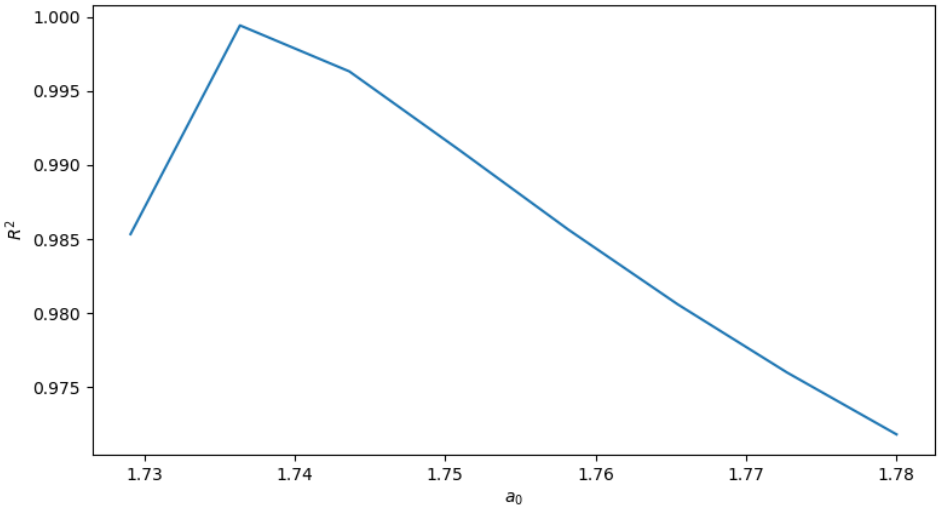

Figure 4: R^2 value of the fit of $\log(1- < h(t;L) > /(a_0 L)$ plotted against $\log L$ plotted for different values of a_0. R^2 is used as a measure of how good the linear fit it, such that the maximum value $a_0 = 1.736 \pm 0.007$, gives the best estimate of a_0.

follows a power law in L. The power was estimated from the gradient of the log-log plot, yielding the estimate of $\sigma_h \sim L^{0.241 \pm 0.002}$.

In the limit $L \to \infty$, the average slope can be found by rearranging Equation 5 $\sigma_z \sim L^{0.759 \pm 0.002}$

$$\langle z(L) \rangle = \frac{\langle h(t;L) \rangle}{L}. \tag{15}$$

Propagating the errors, yields an estimate of the standard deviation of the slope

$$\sigma_{\langle z \rangle}(L) = \frac{\sigma_h(L)}{L}. \tag{16}$$

Therefore, σ_z should also follow a power law and be given by

$$\sigma_{\langle z \rangle}(L) \sim L^{0.241 \pm 0.002 - 1} = L^{-0.759 \pm 0.002} \tag{17}$$

Figure 7 verifies this relationship, where $\sigma_z(L) \sim L^{-0.759 \pm 0.002}$. As a consequence, $\sigma_z \to 0$ as $L \to \infty$. By combining Equation 15 and 13, it can be seen that $\langle z \rangle \to a_0$ as $L \to \infty$.

2.g Height probability distribution

The height probability $P(h;L)$ is defined as the number of configurations with height h in pile of size L divided by the total configurations. To find its distribution, we consider the height of the pile

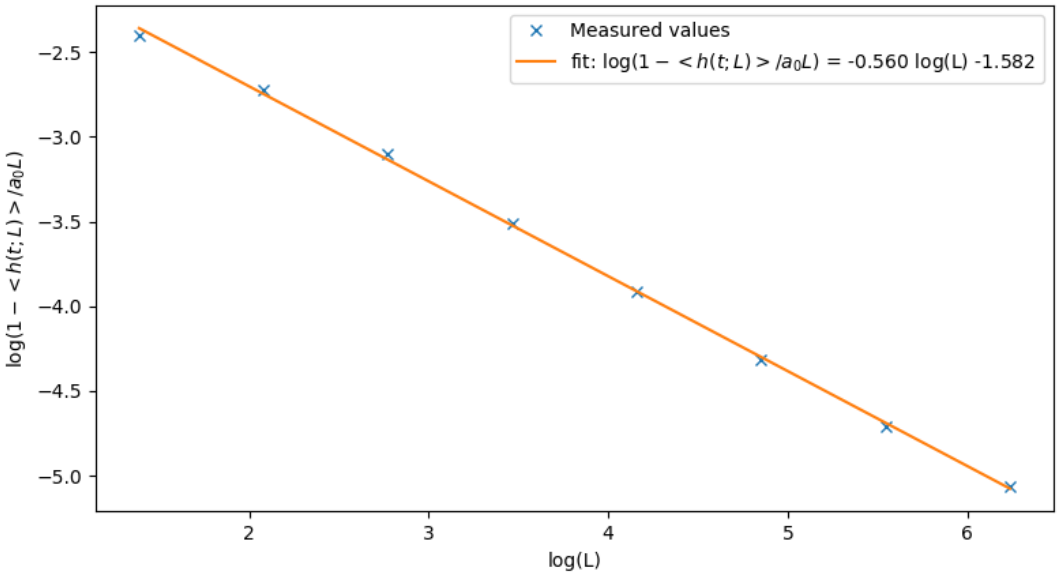

Figure 5: The measured values of $\log(1- < h(t;L) > /(a_0 L)$ plotted against $\log L$, using $a_0 = 1.736$.

$$h = \sum_{i=1}^{L} z_i. \tag{18}$$

Assuming that z_i are independent, identically distributed random variables with finite variance. Then for $L>>1$, CLT predicts that z_i is normally distributed, and thus as $P(h;L)$ is a sample of z_i, it is also normally distributed. Therefore we can use a Gaussian distribution for $P(h;L)$

$$P(x|\mu,\sigma) = \frac{1}{\sqrt{2\pi\sigma}} \exp\left[-\frac{(x-\mu)^2}{2\sigma^2}\right] \tag{19}$$

for the height of the pile, the parameters are given by $\sigma = \sigma_h(L), \mu = \langle h(t;L)\rangle$ and $x = h$

$$\sqrt{2\pi}\sigma P\left(h|\langle h(t;L)\rangle, \sigma_h(L)\right]\sigma_h(L) = \exp\left[-\frac{h - \langle h(t;L)\rangle_t}{2\sigma_h^2(L)}\right] \tag{20}$$

The Gaussian nature of the probability is verified in Figure 8, where the height probability is plotted for different system sizes. From Equation 20, the scaling function $\mathcal{G}(x)$ can be identified

$$\mathcal{G}(x) = \exp\left(-\frac{x^2}{2}\right). \tag{21}$$

which means that we can produce a data collapse by plotting $\sqrt{2\pi}\sigma_h(L)P(h;L)$ vs $(h-\langle h(t;L)\rangle)/\sigma_h(L)$. To check how well the Gaussian approximation holds, Figure 3 have plotted the LHS divided by the RHS of Equation 20, as a function of $(h - \langle h(t;L)\rangle)/\sigma_h(L)$. A perfect agreement with the theoretical Gaussian distribution would result in a line of y

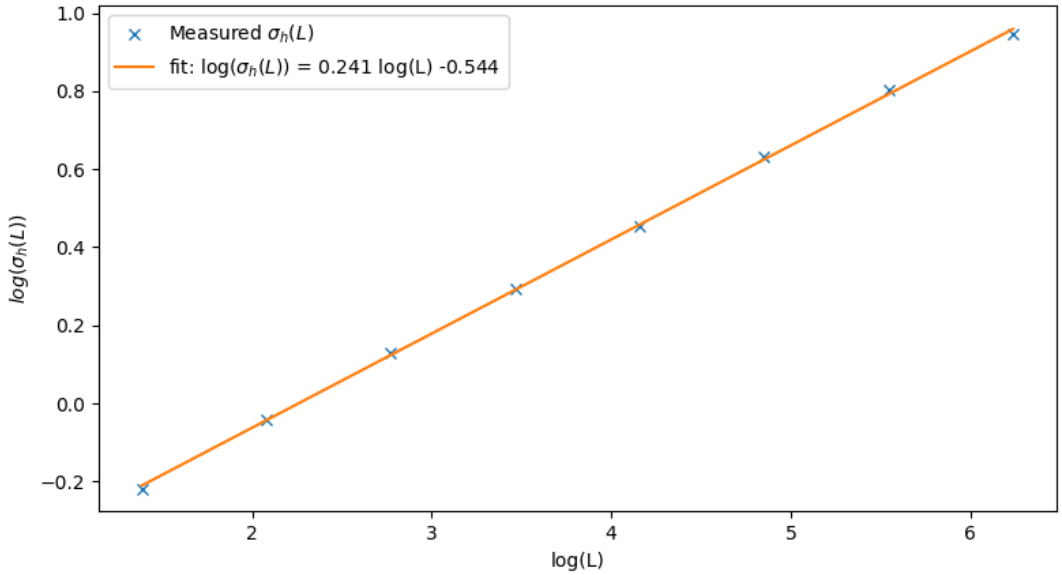

Figure 6: Showing $\sigma_h vs L$, plotted on a log-log scale to find the power of the function.

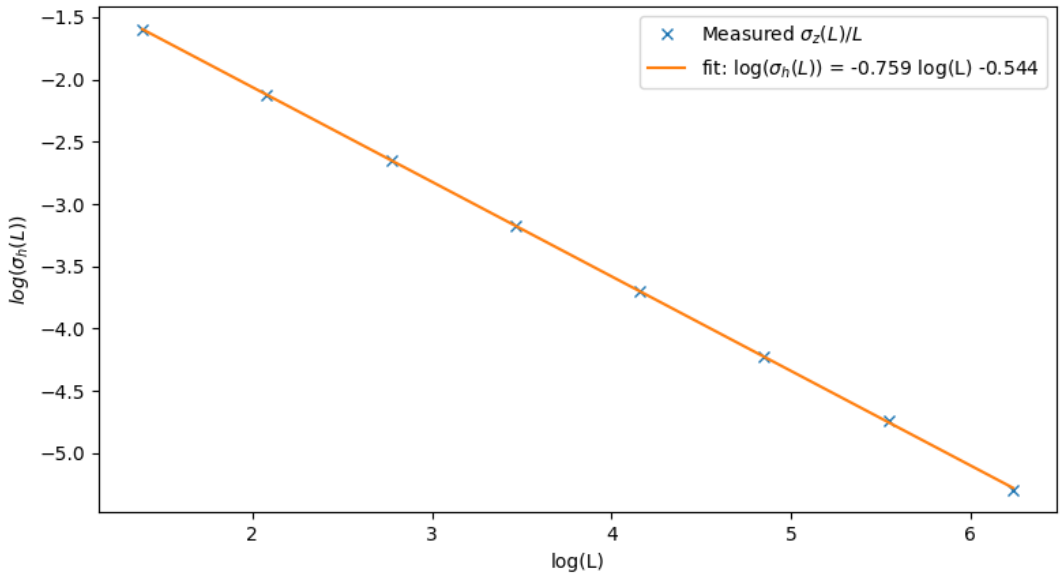

Figure 7: Showing $\sigma_z vs L$, plotted on a log-log scale to find the power of the function.

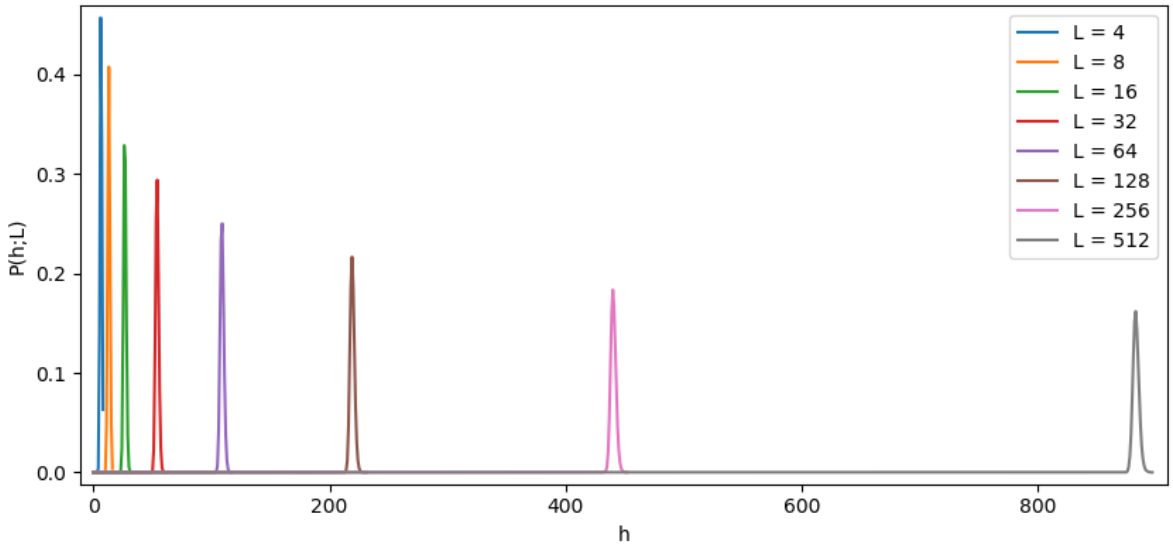

Figure 8: Plot showing the height probability function for different system sizes. The distribution have some resemblence of a Gaussian distribution, that is centred at the average height.

= 1. It can be seen that the measured result clearly deviates from the line, but at heights near the average height, the Gaussian approximation is fairly accurate. The lower than expected value for negative x-values and higher than expected values for positive x-values, illustrates that the measured data are skewed towards the positive x-direction. The Gaussian approximation is most accurate for large system sizes, as you would expected from CLT.

The assumption that z_i are independent, identically distributed random variables with finite variance, that led to the Gaussian approximation means that the σ_h must follow the equation for standard deviation

$$\sigma = \sqrt{\frac{1}{L}\sum_{i=1}^{L}(x_i - \mu)^2}. \tag{22}$$

Assuming that z_i are independent and randomly distributed leads to the relation

$$\sigma_{\langle z \rangle}(L) \propto \frac{1}{\sqrt{L}}, \tag{23}$$

recalling that $\sigma_{\langle z \rangle}(L) = \sigma_h(L)/L$, leads to the expression

$$\sigma_h = L\sigma_z(L) \propto \sqrt{L}. \tag{24}$$

This result deviates from the power law found in section g of $\sigma_h \sim L^{0.241 \pm 0.002}$. This arises from the fact that z_i is not independent near the boundaries, as different scaling relations apply here [5].

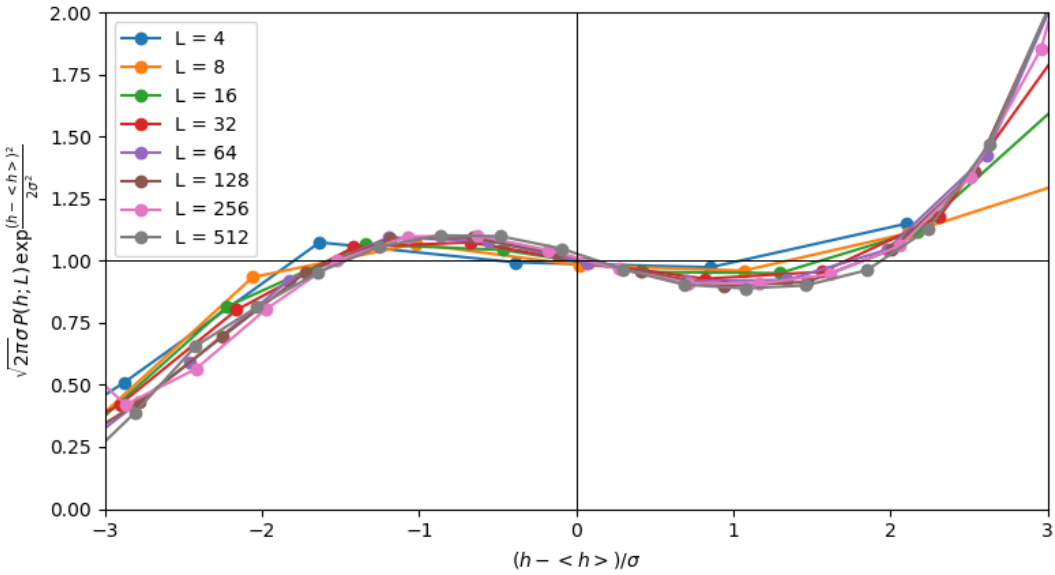

Figure 9: A plot to examine the accuracy of using a Gaussian approximation for a data collapse. The LHS divided by the RHS of Equation 20 is plotted as a function of $(h - \langle h(t;L)\rangle)/\sigma_h(L)$. A perfect agreement would be represented by a line at y = 1. The division by an exponential, makes the function blow up away from x = 0. The measured data is skewed in the positive direction.

3 The Avalanche-size Probability

3.a Avalanche-size probability

The avalanche size s, is defined as the total number of relaxations initiated by adding a grain at site $i = L$. In this section we will study the avalanche-size probability and associated moments, for systems in the recurrent configurations. The avalanche-size probability $P(s;L)$ is defined as the number of avalanches of size s in a system of size L, divided by the total number of avalanches. Since $P(s;L)$ decays like a power law, large avalanches has poor statistics, that causes a noise tail in $P(s;L)$ [5]. Data binning can, in this case, be used to extract information about the noise tail of $P(s;L)$, where the statistics are poor. The data is binned by dividing the s-axis into bins labelled $j = 0, 1, \ldots,$ where the jth bin covers the interval $[a^j, a^{j+1}]$. With $a > 1$, the bins are exponentially increasing in length.

$$\tilde{P}_N(s^j;L) = \frac{\text{No. of avalanches in bin } j}{N\Delta s^j} \tag{25}$$

where Δs^j is the number of integers in the interval and s^j is the geometric mean of the avalanche sizes in bin j. Note that there is no one-to-one correspondence between $P_N(s;L)$ and $\tilde{P}_N(s^j;L)$. Figure 10 illustrates the effect of binning the avalanche-size probability data for a system size $L = 512$ with 10^6 drives and $a = 1.3$. The value of $a = 1.3$ was found to be the best compromise between being high enough to clean up the data, while also minimising loss of information from the probability distribution.

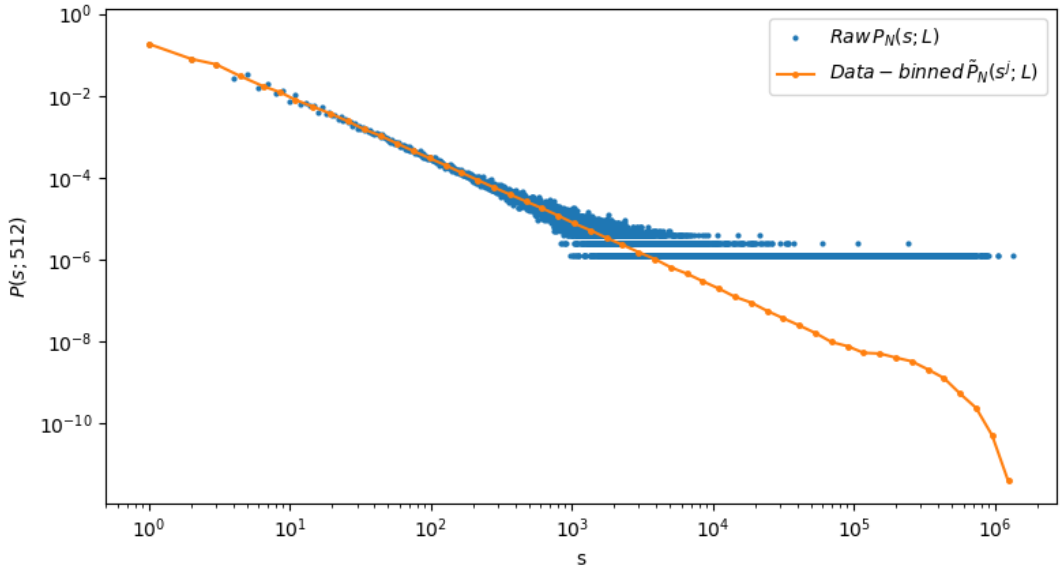

Figure 10: The figure illustrates the effect of data-binning the avalanche-size probability. The log-binned $\tilde{P}_N(s^j;L)$ is shown in orange and the raw $P_N(s;L)$ shown blue points. The data was measured for a system size $L = 512$, for 10^6 runs and $a = 1.3$. The data-binning extracts information of the noise tail, which reveals the finite cutoff avalanche size.

Figure 11 shows the data-binned avalanche-size probability for different system sizes. All the system sizes follows a straight line to begin with on the log-log plot, until bumping upwards, followed by a rapid decline. The bump is a result of the finite system size, as the size of the avalanche is limited by the system size, such that it piles up in a collection of system spanning avalanches. The finite cutoff avalanche size, is also result of the finite system size.

3.b Finite-size scaling ansatz

From Figure 11, we can see that the avalanche-size probability is independent to begin with and decays exponentially with s. When the probability reaches the bump, it is dependent on system size again. All the bumps are evenly distributed, with about equal sizes. With this in mind, a Finite-Size Scaling (FSS) ansatz can be proposed [3]

$$\tilde{P}_N\left(s^j;L\right) \propto s^{-\tau_s}\mathcal{G}\left(s/L^D\right) \qquad \text{for } L \gg 1, s \gg 1 \tag{26}$$

where τ_s is the avalanche-size exponent and D the avalanche dimension. To verify the FSS, a data collapse of the avalanche.size probability can be made by plotting $\tilde{P}_N\left(s^j;L\right)s^{\tau_s}$ vs s/L^D. To perform the data collapse, we first need to estimate τ_s and D. First, t_s controls the height of the bumps and can be found by lining up all the bumps, as shown in Figure 12. The ideal value was found to be $\tau_s = 1.53$. Similarly, D can be estimated by aligning the peak position horizontally. Using the ideal value of $D = 2.18$ and $\tau_s = 1.53$, the final data collapse is shown in Figure 13. As they all collapse onto a line, we can

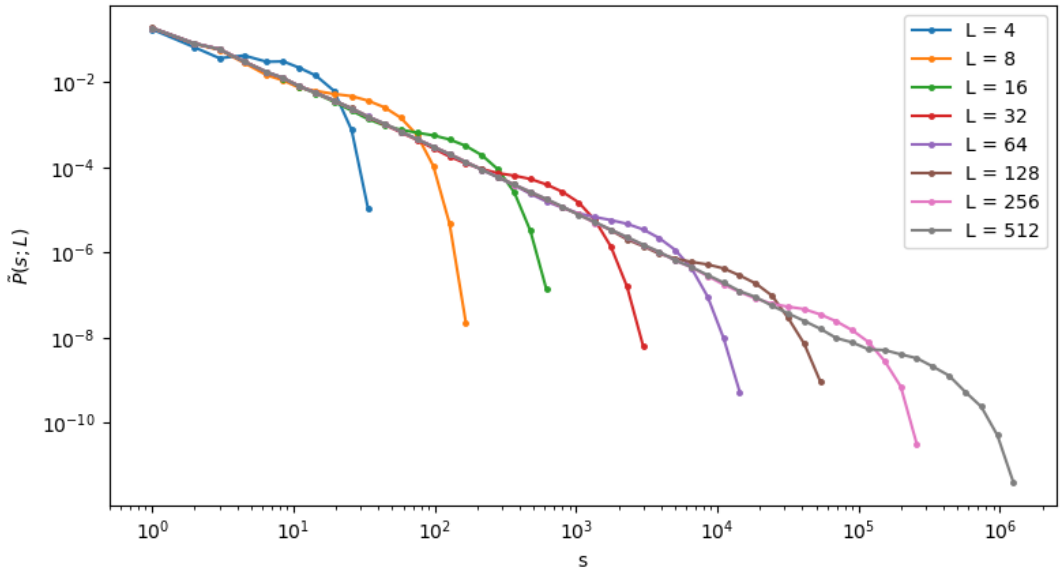

Figure 11: The data-binned avalanche-size probability for various system sizes, measured for 10^6 runs and $a = 1.3$. The finite cutoff avalanche-size increases with system size L.

assume that the FSS ansatz is a good representations of the avalanche-size probability. System size $L = 4$, deviates from the others, as the finite system is most prevalent here.

3.c Moment analysis

Finally, we investigate the k^{th} moment of the avalanche-size, which is given by

$$\langle s^k \rangle = \lim_{T\to\infty} \frac{1}{T} \sum_{t=t_0+1}^{t_0+T} s_t^k \tag{27}$$

where s_t is the measured avalanche size at time t and $t_0 > t_c$, such that the system is in its steady state configurations. The measured k^{th} moments for $k \in \{1, 2, 3, 4, 5\}$ are plotted in Figure 14. It shows that on the log-log plot, s^k scales linearly with L. Corrections to scaling can be seen from the deviation from the straight line, especially for large k values.

To find the relationship between s^k and L, we can write $\langle s_k \rangle$ in terms of the avalanche-size probability distribution [5]

$$\langle s^k \rangle = \sum_{s=1}^{\infty} s^k P(s; L) \tag{28}$$

assuming that the FSS function proposed in section b holds, this can be rewritten as

$$\langle s^k \rangle = \sum_{s=1}^{\infty} s^{k-\tau_s} \mathcal{G}\left(s/L^D\right) \tag{29}$$

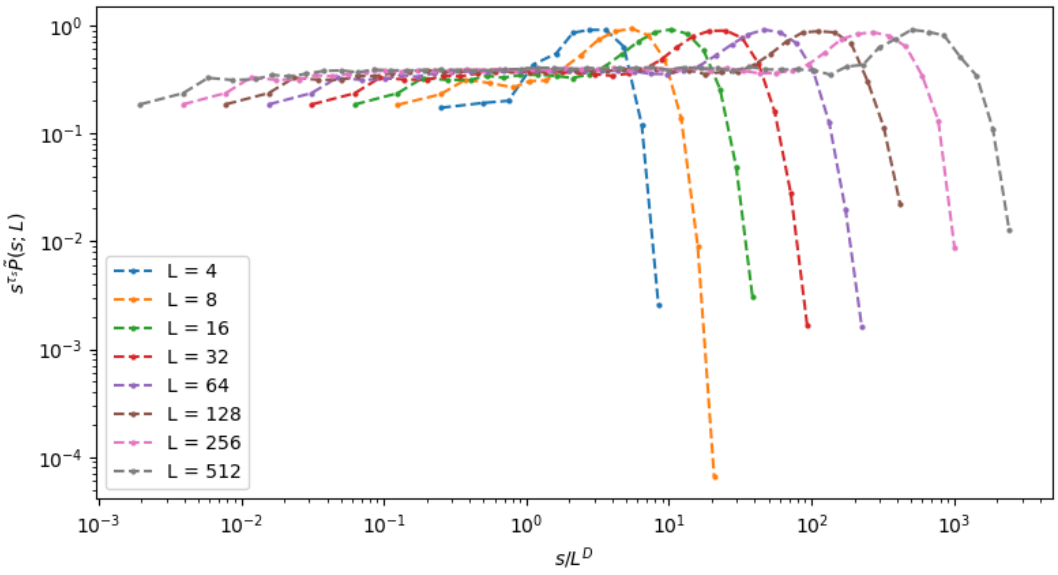

Figure 12: Estimating τ_s by scaling height of the bumps, by setting $D = 1$ and finding the value of τ_s that aligns the bumps vertically. Found to be $\tau_s = 1.53$.

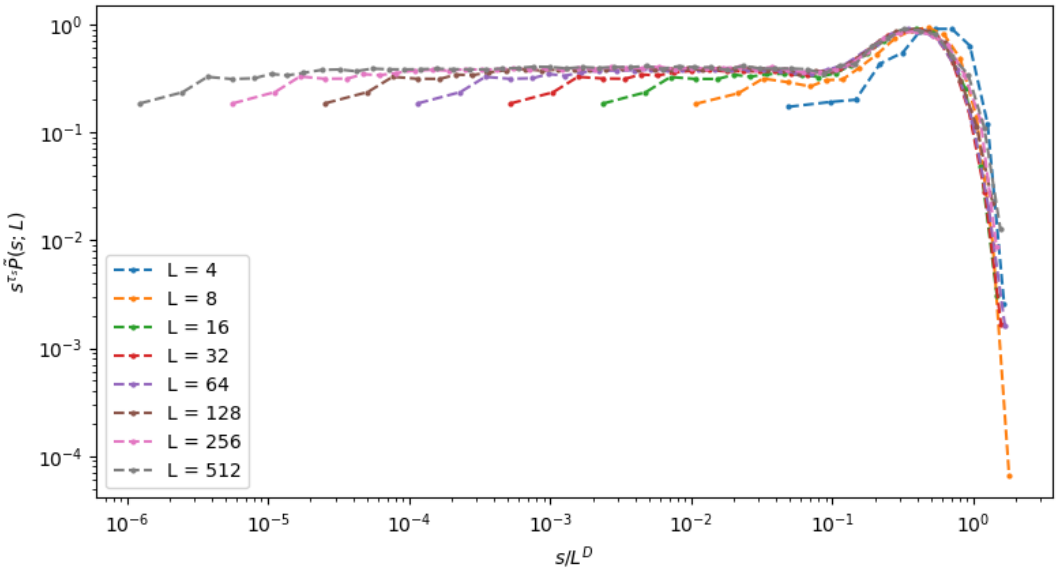

Figure 13: Data collapse of the avalanche-size probability, using the proposed FSS ansatz with the parameters $\tau_s = 1.53$ and $D = 2.18$. Since the the scaling relation collapses the data onto a line, we can assume that the FSS is valid. Finite system size limitations can be seen for $L = 4$.

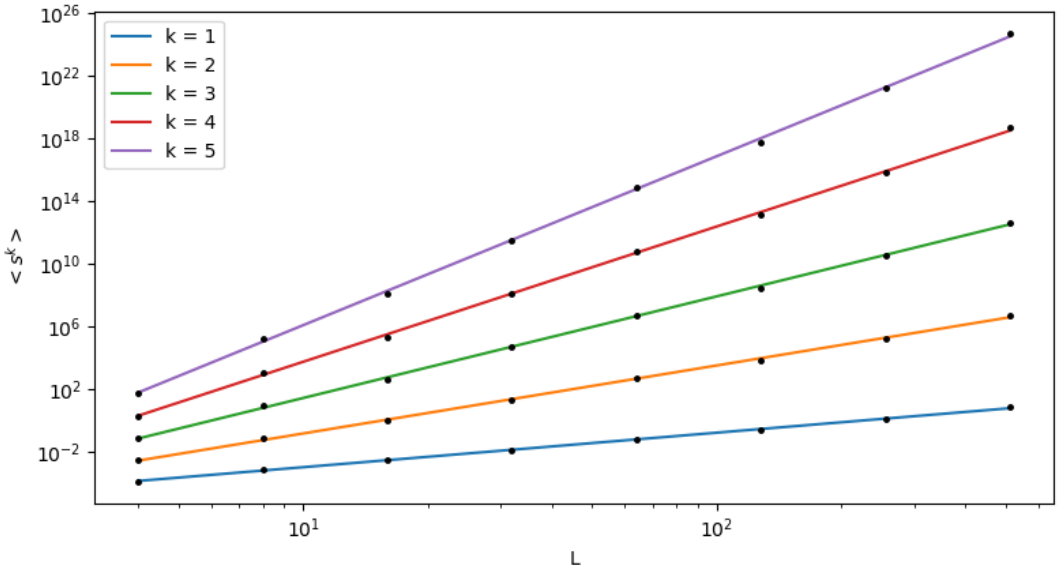

Figure 14: Plot of the k^{th} moment for $k = 1, 2, 3, 4, 5$. The lines represents a linear fit of each k^{th} moment. Corrections to scaling can be seen in deviations from the straight line, especially for large k.

approximating the sum as an integral and using the substitution $u = s/L^D$, the k^{th} moment can be approximated as

$$\langle s^k \rangle \propto L^{D(1+k-\tau_*)} \int_{1/L^D}^{\infty} u^{k-\tau_s} \mathcal{G}(u) du \qquad u = s/L^D. \tag{30}$$

This approximation requires $L>>1$, as the main contributions are from $s>>1$ and the lower limit is approximated as 0 [5]. These corrections for scaling were observed in Figure14, for small system sizes and large values of k. If the avalanche-size exponent satisfies $1 + k > \tau_s$, the integral will converge in the lower limit. From Figure 13, it can be seen that $\mathcal{G}(u)$ decays rapidly for $L>>1$, and so it must also converge in the upper limit. Therefore, as $L \to \infty$, the integral must tend towards a constant, such that we can write

$$\left\langle s^k \right\rangle \propto L^{D(1+k-\tau_s)} \quad \text{for } L \gg 1, k \geq 1 \tag{31}$$

By taking the logarithm of both sides, we can estimate D and τ_s from the gradient of $\log(\langle s^k \rangle)$ vs $\log(L)$. Figure 15 shows the gradient of each k moment in Figure 14 plotted against k. From Equation 31, the gradient of this line can be used to estimate D and τ_s, yielding the values $D = 2.15 \pm 0.01$ and $\tau_s = 1.58 \pm 0.01$. Figure 15 did not show any corrections to scaling, as all the points lie on the straight line.

4 Conclusion

In conclusion, the implemented model displayed self-organised criticality. Several investigations were performed to find the average scaling in height, slope and height probability

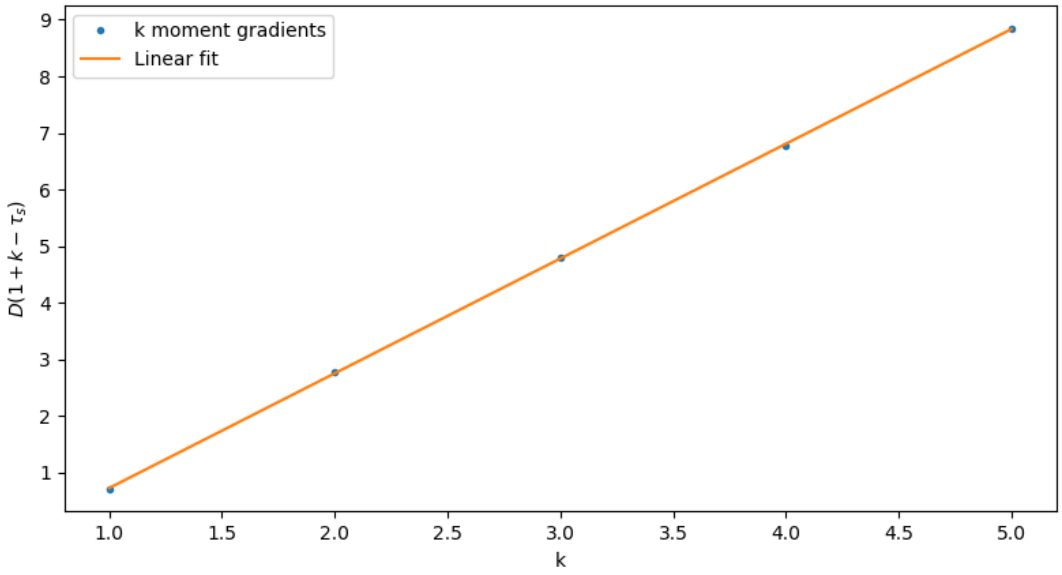

Figure 15: The gradient of the k^th moment, plotted against k, which is used to estimate D and τ_s from the linear fit.

distribution. These relationships were used to perform a data collapse. Corrections to scaling was seen for small system sizes.

The avalanche-size probability was found and used to perform a data collapse with a scaling function, giving the parameters $D = 2.18 \pm 0.01$ and $\tau_s = 1.53 \pm 0.01$. Finally, the k^{th} moment of the avalanche size was found and used to estimate the scaling function parameters, giving the new values: $D = 2.15 \pm 0.01$ and $\tau_s = 1.58 \pm 0.01$, which is consistent with the previous values with a 1.4% and 3.3% deviation, respectively.

References

[1] Frette, V., et al. "Avalanche dynamics in a pile of rice." Nature 379.6560 (1996):

[2] K. Christensen, A. Corral, V. Frette, J. Feder, and T. Jøssang, Tracer dispersion in a self-organized critical system, Phys. Rev. Lett. 77, 107–110 (1996)

[3] K.Christensen, Complexity project notes, Imperial College London (2020)

[4] G. Pruessner, Self-organised Criticality, Cambridge University Press (2012)

[5] K. Christensen and N. Maloney, *Complexity and Criticality*, Imperial College Press, London, (2005).